

Article

Split-Band Interferometry-Assisted Phase Unwrapping for the Phase Ambiguities Correction

Ludivine Libert ^{1,*} , Dominique Derauw ¹, Nicolas d'Oreye ^{2,3}, Christian Barbier ¹ and Anne Orban ¹

¹ Centre Spatial de Liège, Université de Liège, Avenue du Pré-Aily, B-4031 Angleur, Belgium; dderaaw@ulg.ac.be (D.D.); cbarbier@ulg.ac.be (C.B.); aorban@ulg.ac.be (A.O.)

² European Centre for Geodynamics and Seismology, Rue Josy Welter 19, L-7256 Walferdange, Grand-Duchy of Luxembourg; ndo@ecgs.lu

³ National Museum of Natural History, Rue de Munster 25, L-2160 Luxembourg, Grand-Duchy of Luxembourg

* Correspondence: llibert@ulg.ac.be; Tel.: +32-4-372-47-01

Received: 20 July 2017; Accepted: 19 August 2017; Published: 23 August 2017

Abstract: Split-Band Interferometry (SBInSAR) exploits the large range bandwidth of the new generation of synthetic aperture radar (SAR) sensors to process images at subrange bandwidth. Its application to an interferometric pair leads to several lower resolution interferograms of the same scene with slightly shifted central frequencies. When SBInSAR is applied to frequency-persistent scatterers, the linear trend of the phase through the stack of interferograms can be used to perform absolute and spatially independent phase unwrapping. While the height computation has been the main concern of studies on SBInSAR so far, we propose instead to use it to assist conventional phase unwrapping. During phase unwrapping, phase ambiguities are introduced when parts of the interferogram are separately unwrapped. The proposed method reduces the phase ambiguities so that the phase can be connected between separately unwrapped regions. The approach is tested on a pair of TerraSAR-X spotlight images of Copahue volcano, Argentina. In this framework, we propose two new criteria for the frequency-persistent scatterers detection, based respectively on the standard deviation of the slope of the linear regression and on the phase variance stability, and we compare them to the multifrequency phase error. Both new criteria appear to be more suited to our approach than the multifrequency phase error. We validate the SBInSAR-assisted phase unwrapping method by artificially splitting a continuous phase region into disconnected subzones. Despite the decorrelation and the steep topography affecting the volcanic test region, the expected phase ambiguities are successfully recovered whatever the chosen criterion to detect the frequency-persistent scatterers. Comparing the aspect ratio of the distributions of the computed phase ambiguities, the analysis shows that the phase variance stability is the most efficient criterion to select stable targets and the slope standard deviation gives satisfactory results.

Keywords: synthetic aperture radar; interferometry; phase unwrapping; split-band; multichromatic analysis

1. Introduction

Over the years, performances of Synthetic Aperture Radar (SAR) sensors have been improved to finally reach the metric resolution by combining the synthetic aperture principle in the azimuth direction with an increase of the radar signal bandwidth in the range direction. Using such data, the well-known SAR Interferometry (InSAR) solves the relationship between the phase and the optical path difference to retrieve the topography. However, the spectral information of the range component is rarely exploited. Split-Band Interferometry (SBInSAR), also known as Multichromatic

Analysis, exploits the information contained in the frequency domain to put an added value to SAR Interferometry. It applies InSAR to subrange images obtained by splitting the large available range bandwidth of recent sensors and explores the phase trend through the partial interferograms in order to provide pointwise absolute phase measurements. This process is equivalent to an absolute and spatially independent phase unwrapping, as long as it is performed on scatterers with a stable behaviour across the spectral domain. Such targets are called frequency-persistent scatterers (PS_f) [1]. The theoretical applicability of Split-Band Interferometry and its performance regarding the spectral decomposition parameters are discussed in [2]. This work showed that the quality of the split-band phase is the result of a trade-off between increasing the number of subbands of the spectral decomposition and preserving a sufficient resolution for the subrange images [2]. The practical feasibility of topographic measurements has been reported in [3] for airborne data in X-band with a total bandwidth of 400 MHz. The study in [1] applied the technique to spaceborne TerraSAR-X data in spotlight mode (300 MHz) over the Uluru monolith in Australia. The same test site has been considered by [4] using Cosmo-SkyMed images with a total bandwidth of 325 MHz. Another study [5] also demonstrated the potential of SBInSAR for height retrieval using a TanDEM-X bistatic pair of images of 100 MHz bandwidth over Nyiragongo volcano, but stressed the need for a larger value of the initial range bandwidth. So far, the frequency-persistent scatterers have been selected using the multifrequency phase error [6] that is an estimator of the coherence from one spectral subband to another and that quantifies the quality of the phase measurements. In [7], the scattering properties of the frequency-persistent scatterers and "temporally" coherent scatterers (PS) from the Permanent Scatterers Interferometry (PSI) [8] are investigated. Among the potential applications of SBInSAR, let us mention absolute height retrieval, change detection [9], ionospheric correction [10,11] and urban monitoring. The spectral diversity of the range bandwidth can also be used to improve coregistration as discussed in [12] or to estimate high-gradient surface displacements, such as earthquake ruptures [13].

Most InSAR phase unwrapping algorithms are aimed to perform relative measurements and determine the phase of a pixel with respect to the phase of its neighbours, rather than the absolute phase. It is a real issue in practice because noncoherent patches due to geometrical distortions (layover, shadowing) or time changes can isolate coherent regions from each other and cause a separate phase unwrapping from one region of the interferogram to another. This introduces unknown phase ambiguities and prevents from comparing the phase between two separated regions. Because SBInSAR provides absolute phase measurements, it can potentially solve these phase ambiguities and reconnect the phase of distinct regions. Since we only need to know the integer number of cycles that must be added to the wrapped phase to solve the phase ambiguities, the accuracy requirements regarding the split-band phase are less demanding than in the case of height retrieval.

In this study, we propose an approach based on SBInSAR to complement the InSAR phase unwrapping that estimates and corrects the phase ambiguities, and we demonstrate its efficiency. In Section 2, we set the basic notions and equations of Split-Band Interferometry and we present the method for the phase ambiguities correction. We also propose new methods to select robust PS_f . In Section 3, the SBInSAR-assisted phase unwrapping is tested on spotlight images acquired over Copahue volcano. The test site is described, as well as the data set and the processing. An indirect validation procedure is also presented, along with an indicator to compare the precision of the results.

2. Methods

Split-Band Interferometry is a three-step process derived from classical SAR Interferometry. It takes advantage of the large range bandwidth of recent SAR sensors to work the absolute interferometric phase out. The splitting of the range bandwidth of a SAR scene into several narrower subbands produces lower resolution images of this scene, each one with a frequency slightly shifted with respect to the initial one. During the first step of the SBInSAR process, the same spectral decomposition is applied to the already coregistered master and slave images of a given interferometric pair. In a second step, interferometry is performed on each pair of master and slave subimages. It yields

a set of interferograms where the pointwise phase evolves linearly across the spectral domain. The slope of the final pixel-by-pixel linear regression of the phase is proportional to the absolute optical path, and it therefore enables performing absolute phase measurements on the points considered as spectrally stable targets.

The operating and rationale of the SBInSAR processor have already been presented in [5]. In this section, we will first outline the basic principles of Split-Band Interferometry and the corresponding equations. We will then define the estimators for the characterization and detection of frequency-persistent scatterers. Finally, we will present our approach for the phase-offset determination.

2.1. Rationale of Split-Band Interferometry

Let us consider an interferometric pair of coregistered images with a bandwidth B and a carrier frequency ν_0 . They are spectrally decomposed into N subbands of partial bandwidth B_N centered at frequencies ν_i ($i = 1, 2, \dots, N$), N being odd. Frequencies of adjacent subbands are shifted of $\Delta\nu$. As stated in [5], the interferometric phase of the coregistered and spectrally decomposed images in the i^{th} partial interferogram is expressed by:

$$\Delta\phi_i = \frac{4\pi}{c}(r_s - r_m - e_c)\nu_0 + \frac{4\pi}{c}e_c\nu_i, \quad (1)$$

where r_m and r_s are the range coordinates in master and slave images, respectively, e_c is the coregistration error and the dependence on the coordinates of the pixel is implicit for the sake of clarity. The phase behavior of a point across the N partial interferograms is fitted by a simple linear function:

$$p(\nu_i) = s\nu_i + u, \quad (2)$$

where s and u are the fit parameters. The slope of this linear regression is given by:

$$s = \frac{\partial(\Delta\phi_i)}{\partial\nu_i} = \frac{4\pi}{c}e_c. \quad (3)$$

In this case, the absolute optical path difference is the sum of the registration Δr applied on the range coordinate and the coregistration error e_c . The phase issued by the split-band process, called the split-band phase, is therefore computed as:

$$\begin{aligned} \Delta\varphi &= \Delta\varphi_{reg} + \Delta\varphi_{e_c} \\ &= \frac{4\pi}{c}\nu_0\Delta r + \frac{4\pi}{c}\nu_0e_c. \end{aligned} \quad (4)$$

Nevertheless, the split-band phase measurement can only be considered as absolute if it is known with a sufficient accuracy. Since the second term of Equation (4) is obtained by multiplying the slope of the linear regression by the initial carrier frequency, the accuracy of the split-band phase is directly related to the accuracy of slope through:

$$\sigma_{\Delta\varphi} = \nu_0\sigma_s, \quad (5)$$

with $\sigma_{\Delta\varphi}$ being the standard deviation of the split-band phase and σ_s the standard deviation of the slope coefficient s of the linear regression. Considering the chi-square fitting of a straight line, the latter can be expressed as follows:

$$\sigma_s = \frac{1}{\Delta\nu} \sqrt{\frac{\sum_{i=1}^N \frac{1}{\sigma_{\phi_i}^2}}{\sum_{i=1}^N \frac{1}{\sigma_{\phi_i}^2} \sum_{i=1}^N \frac{x_i^2}{\sigma_{\phi_i}^2} - \left(\sum_{i=1}^N \frac{x_i}{\sigma_{\phi_i}^2}\right)^2}}, \quad (6)$$

where x_i is the subband index ranging from $-\frac{N-1}{2}$ to $\frac{N-1}{2}$ and $\sigma_{\phi_i}^2$ is the phase variance in the i^{th} partial interferogram. This expression holds for independent data points, i.e., nonoverlapping subbands.

2.2. Detection of Frequency-Persistent Scatterers

The linearity of the phase assumed in Equation (1) holds only for targets with a coherent behavior across the spectral domain, i.e., for frequency-persistent scatterers. The consequence is that the stable nature of a frequency-persistent scatterer insures the accuracy of the split-band phase measurement, and it is therefore fundamental to correctly detect PS_f.

In the following, we define the multifrequency phase error that is the commonly used criterion to detect spectrally stable targets, and we propose two new detection criteria: the slope standard deviation and the phase variance stability. These new criteria are meant to improve the selection of the PS_f population and their efficiency will be compared to the one of the multifrequency phase error when applied to the test case.

2.2.1. Multifrequency Phase Error

So far, most studies have exploited the multifrequency phase error σ_v to detect stable targets. This estimator of the split-band phase quality is basically the a posteriori uncertainty of the phase value in the partial interferograms, and it is mathematically defined as:

$$\sigma_v = \sqrt{\frac{1}{N-2} \sum_{i=1}^N (\Delta\phi_i - p(v_i))^2}. \quad (7)$$

2.2.2. Slope Standard Deviation

In the framework of the phase ambiguities retrieval, the split-band phase must be measured with accuracy better than a cycle, and we use this one-cycle accuracy to characterize frequency-persistent scatterers. Setting a threshold of 2π in Equation (5) leads us to a first criterion of selection based on the standard deviation of the slope of the linear regression:

$$\sigma_s < \frac{2\pi}{\nu_0}. \quad (8)$$

This criterion only depends on the initial carrier frequency. In X-band, the upper limit of the phase slope standard deviation has a typical value of 0.65 rad/GHz.

2.2.3. Phase Variance Stability

In order to establish the second criterion, which will be referred to as the phase variance stability, let us assume that the spectral decomposition is symmetrical with respect to ν_0 and that the phase variance $\sigma_{\phi_i}^2$ does not vary much from one subband to another. In this case, the squared sum in Equation (6) can be neglected and we can introduce an upper bound $\sigma_{\phi,max}^2$ on the partial phase variance:

$$\begin{aligned}\sigma_s &= \frac{1}{\Delta\nu} \sqrt{\frac{1}{\sum_{i=1}^N \frac{x_i^2}{\sigma_{\phi_i}^2}}} \\ &\leq \frac{\sigma_{\phi,max}}{\Delta\nu} \sqrt{\frac{1}{\sum_{i=1}^N x_i^2}}.\end{aligned}\quad (9)$$

Given the symmetry of the x_i values, the remaining sum in Equation (9) can be developed as the double sum of the $\frac{N-1}{2}$ first squared integers. Inserting the relation (9) into Equation (5) and setting once again a 2π threshold on $\sigma_{\Delta\phi}$, we finally obtain:

$$\sigma_{\phi,max}^2 < \left(2\pi \frac{\Delta\nu}{\nu_0}\right)^2 \frac{N(N+1)(N-1)}{12}.\quad (10)$$

For a given pixel in the stack, if the value of the phase variance is lower than this limit in every partial interferogram, i.e.:

$$\sigma_{\phi_i}^2 < \sigma_{\phi,max}^2 \quad \forall i = 1, 2, \dots, N,\quad (11)$$

then the required accuracy should be insured and the point is considered as being a PS_f . In practice, the spectral decomposition is always symmetrical with respect to the central carrier frequency. For the second assumption, we consider it as verified when the value of $\sigma_{\Delta\phi}$ varies of less than 5% when the squared sum is neglected.

Let us note that the upper bound given by Equation (10) increases as N^3 . This can be interpreted in the following way: for a large number of bands, the partial phase variance can be important as long as its value from one band to another remains consistent. In this case, the split-band phase will be measured accurately anyway. However, increasing the number of subbands reduces the resolution. The key point of the spectral decomposition will be to determine the number of subbands so as to find a trade-off between accuracy and resolution.

It is important to note that the phase variance stability criterion for the selection of frequency-persistent scatterers is quite stringent: due to the assumption that must be satisfied, the number of selected points will be low. Some valid PS_f may even be missed during the selection. However, the accuracy for the selected points is guaranteed, as we will demonstrate with the test case.

2.3. SBInSAR-Assisted Phase Unwrapping

In a conventional InSAR process, phase unwrapping algorithms generally provide relative measurements of the phase. However, due to decorrelation, they frequently fail to unwrap the interferogram as a whole and parts of the image are separately processed, introducing phase ambiguities that prevent from comparing the phase from one region to another.

We present here an approach based on Split-Band Interferometry to determine and correct the local phase ambiguities of the unwrapped phase. We consider the general case where the phase ambiguity is an unknown number of cycles $2\pi n$, with n being an integer. The phase ambiguity has the same value for all the points through a given region of continuously unwrapped phase. In theory, the presence of a single stable target per independent area is sufficient to solve the phase ambiguities. In practice, however, we have to deal with the phase noise and the uncertainties, and it is not possible to determine which scatterer is the most stable. For this reason, we adopt a statistical analysis of the PS_f to derive this integer number of cycles. Let us specify that the phase-offset, or phase ambiguity, denotes the $2\pi n$ -discrepancy. However, we will largely use these terms in the following sections to refer to the number of cycles n alone.

Let us note $\Delta\phi$ the unwrapped phase obtained with the classical phase unwrapping process. For a given PS_f at pixel's coordinates (k, l) in the image, neglecting the noise and the phase unwrapping errors, the unknown number of cycles can be computed as:

$$n(k, l) = \frac{\Delta\varphi(k, l) - \Delta\phi(k, l)}{2\pi}. \quad (12)$$

The SBInSAR-assisted phase unwrapping will consider one region of the phase unwrapping at a time. In a first time, it will select the PS_f of this region based on one of the criteria presented in the previous section. It will then estimate the phase ambiguities using Equation (12) for all the selected pixels and round each of these values to the nearest integer. The rounded value with the largest number of occurrences, i.e., the mode of the distribution, is assumed to be the phase ambiguity we are looking for. Finally, this value is multiplied by 2π and added to the unwrapped phase of all the pixels of the region in order to correct the phase ambiguity. This procedure is repeated for each region separately unwrapped. When the distribution of the rounded phase ambiguities has multiple modes, no correction is applied. Regions with a population below 10 PS_f are not corrected either, since they frequently show multiple modes. The algorithm steps are presented in Figure 1. In the end of the process, an image of the leveled unwrapped phase is provided, showing only the shifted areas. Let us stress that, despite the loss of resolution in the subproducts, this final unwrapped phase image preserves the initial range resolution.

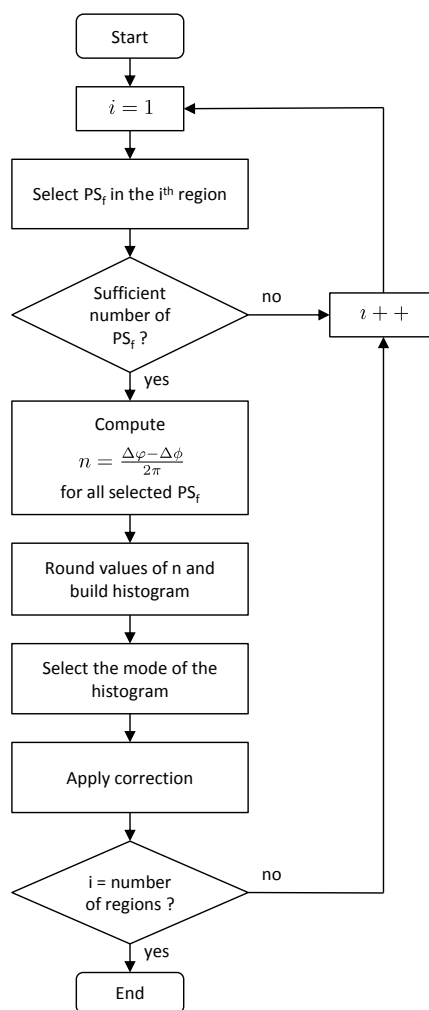


Figure 1. Flow chart of the Split-Band Interferometry-assisted phase unwrapping algorithm.

The routine supports topographic and deformation modes. For both modes, the selection of the stable targets population will be identical, but, in deformation mode, the DEM contribution will be removed from both the unwrapped phase and the split-band phase. Since the offset estimation is based on the difference between these two phases, no difference of performance is expected between topographic and deformation modes, except due to the quality of the unwrapped phase. In the following, we will only consider the topographic mode and no subtraction of the DEM will be made.

Besides, in practice, the rounding of the phase ambiguities to the nearest integer mitigates the influence of the noise and the phase unwrapping error. Although infinitely accurate phase measurements would be necessary in theory, we will show that the one-cycle accuracy assumed for PS_f is enough to determine the phase-offset.

3. Copahue Test Case

3.1. Test Site

Copahue is an active strato-volcano located in the northwest of the Argentinean province of Neuquén in the Andes, at the border between Argentina and Chile (Figure 2a). This volcano has an elongated elliptical shape ($22 \text{ km} \times 8 \text{ km}$) oriented in the SW–NE direction and reaches a maximum elevation of 2997 m. It has nine craters clustered along the $N 60^\circ E$ direction, but only the eastern-most one is active. The active crater is about 300 m deep and contains an acid lake created by abundant precipitations and ice melting [14]. Recent eruptions have been reported in 2000, 2012 and 2014 and the last eruption was accompanied by a degassing unrest [15]. Deformations observed over Copahue volcano using InSAR are discussed in [16,17].

A Google Earth™ (Copahue, Neuquén, Argentina) optical view of the area is given in Figure 2b. The area of interest shows steep topography as well as moderate slopes, little vegetation and a snow cover that can vary over the year. Change in snow cover and frequent precipitations can cause local loss of coherence in InSAR products. Variety of topography, of slope orientations and of geometrical distortions, along with the presence of natural scatterers make Copahue volcano an interesting site to apply SBInSAR-assisted phase unwrapping.

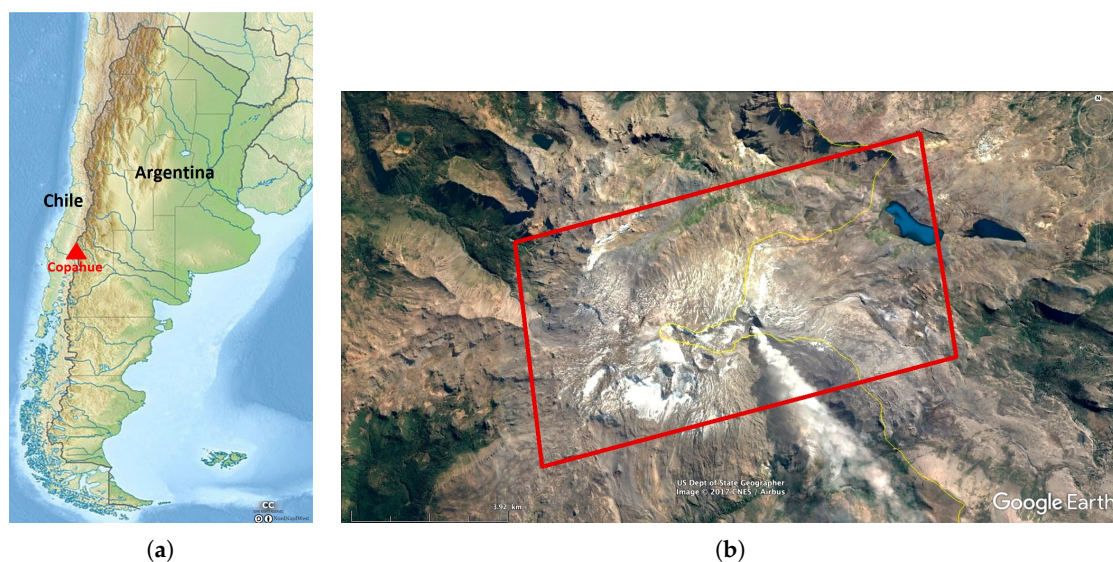


Figure 2. (a) Location of Copahue volcano (red triangle) on the border between Chile and Argentina. (b) Google Earth™ image of Copahue volcano in 2017. The footprint of the InSAR pair is drawn in red.

3.2. Data Set and Processing

The data set used to test the SBInSAR-assisted phase unwrapping method consists in two spotlight images acquired on ascending orbits by TerraSAR-X on 15 and 26 December 2014. Each image is the master image of a pair acquired in pursuit monostatic mode, and the ensemble of both constitutes therefore a standard spotlight interferometric pair. They are acquired in VV-polarization with a look angle ranging from approximately 32.8° to 33.8° and a range bandwidth of 300 MHz. The interferometric pair has a perpendicular baseline of about 32 m that corresponds to a height of ambiguity of 163 m, and a temporal baseline of 11 days, which minimizes the effects of temporal decorrelation.

Studying the deformations over Copahue volcano is outside the scope of the present study, as we wish to make a methodological demonstration only. Therefore, no DEM is used to remove topographic information of the phase during the InSAR processing. Hence, the analyzed signal contains the topography but also possible deformations or artefacts from atmospheric origin.

A multilooking of $5 \text{ pixels} \times 5 \text{ pixels}$ is applied to the images and a coherence threshold of 0.5 is chosen, above which the phase is considered for unwrapping. A branch-cut algorithm is used to unwrap the phase [18]. The coherence map and the corresponding unwrapped InSAR phase are presented in Figure 3. In the coherence map shown in Figure 3a, large decorrelated areas are present in regions corresponding mainly to the snow cover. In Figure 3b, we observe a smooth phase gradient on the main part of the interferogram and numerous smaller regions phase-shifted with respect to the main area.

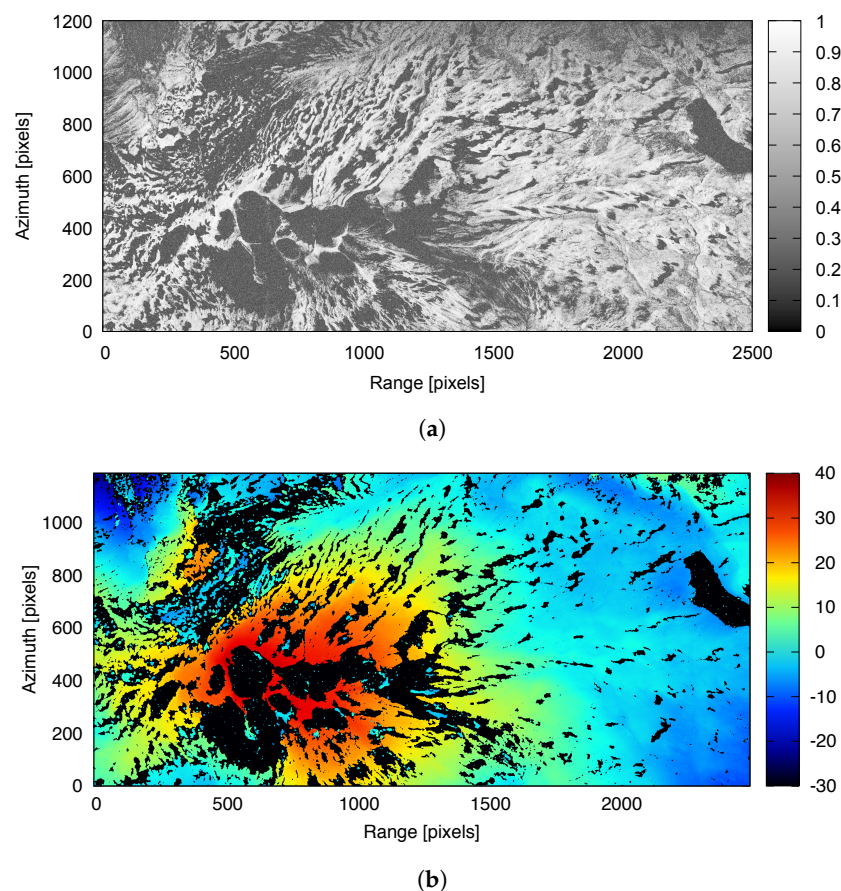


Figure 3. (a) coherence image of the test pair over the Copahue volcano. (b) fully connected unwrapped phase. Color chart values are given in radians.

The SBInSAR processing is applied with a spectral decomposition into five subbands of 60 MHz. Given the 300 MHz initial range bandwidth, the subbands do not overlap and the rationale presented in Section 2 is valid. Moreover, this large partial bandwidth mitigates the resolution loss and therefore insures the quality of the split-band measurements. In the split-band phase image (Figure 4), we observe large patches of noisy phase corresponding mainly to noncoherent areas in the InSAR phase. These noisy patches with high dispersion of values illustrate clearly that all the scatterers are not stable regarding the SBInSAR processing and that the adequate pixels must be selected somehow.

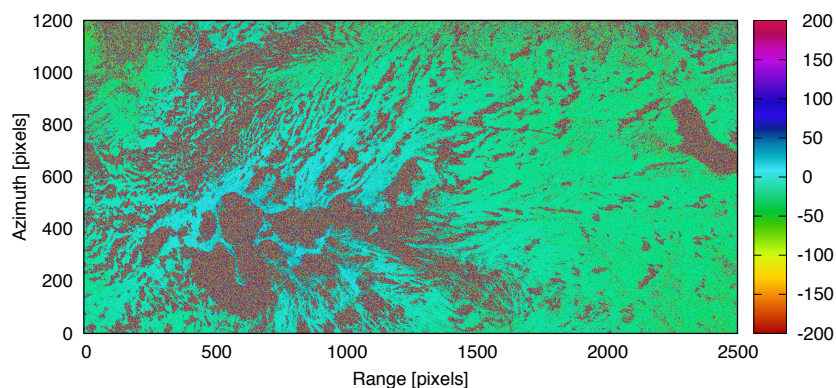


Figure 4. Phase measured with Split-Band Interferometry over Copahue volcano. Color chart values are given in radians.

3.3. Validation Procedure

In order to demonstrate the applicability of the SBInSAR-assisted phase unwrapping without additional measurements, we propose an indirect validation strategy. It consists of disconnecting some regions of the interferogram by introducing artificial cuts during the phase unwrapping process, which is based on a branch-cut method. Knowing the unwrapped phase $\Delta\phi_c$ of the "fully connected" version of the interferogram and the unwrapped phase $\Delta\phi_d$ of the "artificially disconnected" version, and knowing that their values only differ by an entire number of cycles $2\pi m$ with m integer, one can obviously state:

$$m(k,l) = \frac{\Delta\phi_c(k,l) - \Delta\phi_d(k,l)}{2\pi}. \quad (13)$$

This phase-offset will not necessarily be the same as the correction n computed with the SBInSAR-assisted phase unwrapping, but the phase-offset difference between two pixels of coordinates (k_1, l_1) and (k_2, l_2) should be the same for both m and n :

$$n(k_1, l_1) - n(k_2, l_2) = m(k_1, l_1) - m(k_2, l_2). \quad (14)$$

If we focus on pixels in two separate regions, then the relative offset values can be used to validate the results, as illustrated in Figure 5. The artificially disconnected regions of the test pair are shown in Figure 6a. We cut three areas from the main coherent area. The corresponding unwrapped phase is given in Figure 6b. It is obvious from this figure that a phase shift has been introduced for region 2. The relative phase shifts between these regions are listed in Table 1. This will be used in the next section to validate our results.

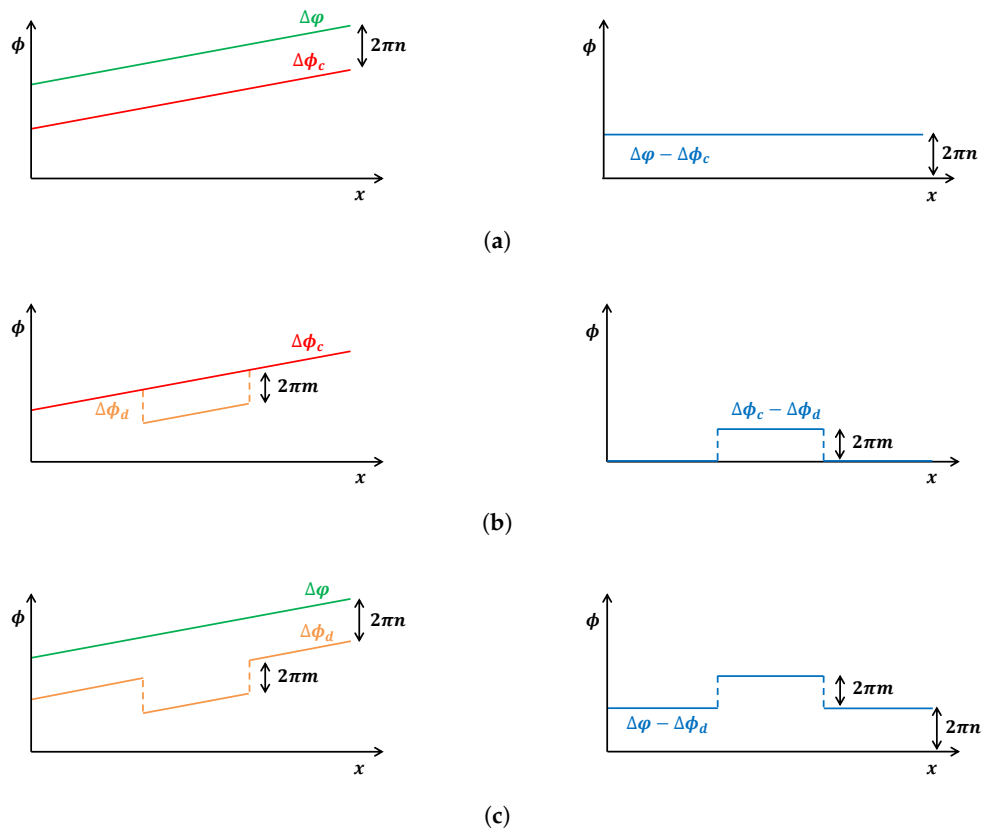


Figure 5. Diagrams of the validation procedure for a one-dimensional simplified interferogram. (a) If the connected InSAR phase $\Delta\phi_c$ is subtracted from the split-band phase $\Delta\phi$, the difference gives an offset $2\pi n$. (b) If a region of the one-dimensional interferogram is disconnected, an offset $2\pi m$ is introduced between the connected phase $\Delta\phi_c$ and the disconnected InSAR phase $\Delta\phi_d$. (c) If the disconnected InSAR phase is subtracted from the split-band phase, the relative offset $2\pi m$ between the disconnected regions remains the same as in case (b).

Table 1. Relative phase-offset values of artificially disconnected regions.

Relative Phase-Offset	Cycles
$m_1 - m_2$	-1
$m_1 - m_3$	0
$m_1 - m_4$	-1
$m_2 - m_3$	1
$m_2 - m_4$	0
$m_3 - m_4$	-1

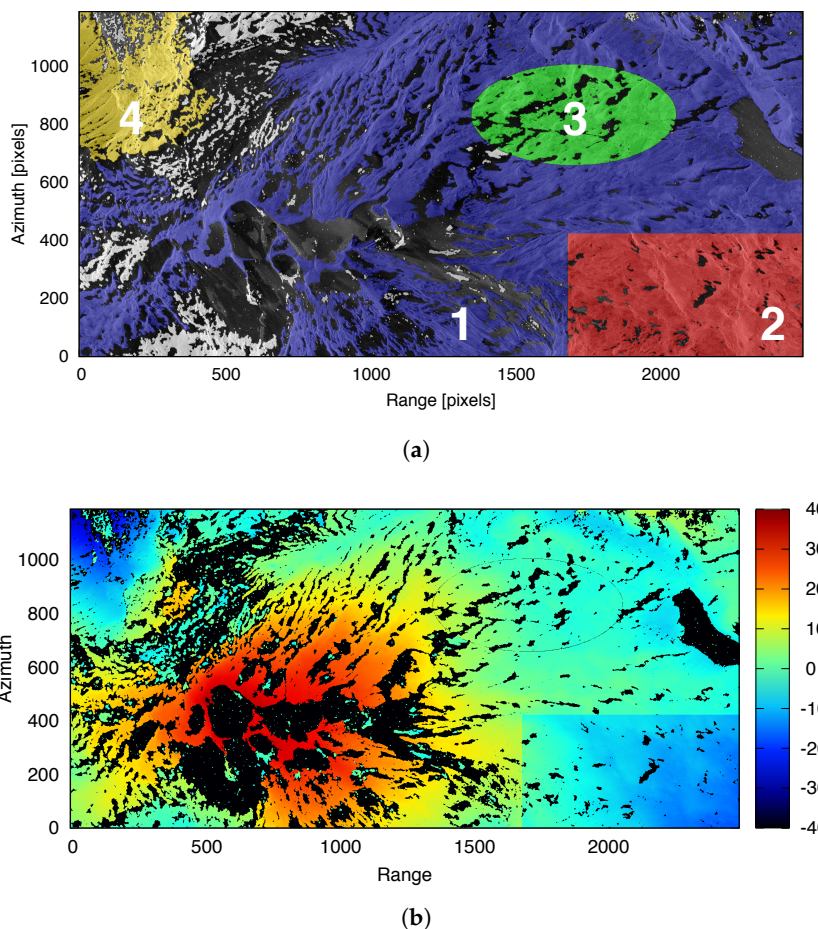


Figure 6. (a) map of the disconnected regions. The main coherent region from which areas have been artificially cut is represented in blue. We refer to the blue region, the red rectangle, the green ellipse and the yellow area, respectively, as the regions 1, 2, 3 and 4. Regions in black are regions with coherence lower than the threshold applied during phase unwrapping. White areas are naturally disconnected parts of the unwrapped phase and they are not considered for the validation of the SBInSAR-assisted phase unwrapping. (b) artificially disconnected version of the unwrapped phase over Copahue volcano. Color chart values are given in radians.

3.4. Indicator of Quality

In the proposed approach for the SBInSAR-assisted phase unwrapping, the phase ambiguity is chosen as the mode of the phase-offsets distribution. The statistical nature of the method makes two requirements necessary in order to have confidence in the correction: first, the probability associated to the mode value must be high; second, the dispersion of the distribution must be low. These two conditions are summarized by a low W/H ratio, W and H being, respectively, the width and the height of the normalized distribution. The normalized distribution of the rounded phase-offsets can be fitted by a normal law:

$$f(n) = \frac{1}{\sigma\sqrt{2\pi}} \exp\left(-\frac{1}{2}\left(\frac{n-\mu}{\sigma}\right)^2\right) \quad (15)$$

with the expectation value μ and the standard deviation σ being the parameters of the fit. The height of the distribution is defined as the maximum of the fitted normal law and the width is characterized by the half width at half maximum. The ratio is then given by:

$$\frac{W}{H} = \frac{\sigma\sqrt{2\ln(2)}}{f(\mu)}. \quad (16)$$

The aspect ratio of the distribution is an indication regarding the precision of the measurement, not its accuracy. It will therefore allow to compare the precision of two different estimations, but it will not assess if the measurement is correct or not.

4. Results and Discussion

In a first time, the SBInSAR-assisted phase unwrapping is applied on the four artificially disconnected areas of the Copahue test case in order to validate the approach for the phase ambiguities correction and determine which detection criterion is the best. Four situations are considered from the PS_f selection point of view: in the initial situation, we do not discriminate the PS_f and keep all the pixels. In the other cases, the PS_f are selected using either the multifrequency phase error σ_v , the threshold on standard deviation of the slope σ_s of the linear regression or the stability of the phase variance $\sigma_{\phi_i}^2$. We set a threshold of 0.5 on the multifrequency phase error. The number of selected pixels according to the region and the detection criterion is shown in Figure 7. Since the first region is noticeably larger than the three others, it shows therefore a larger population of selected pixels for any detection criterion. The number of detected pixels is much higher in the case of the multifrequency phase error than for the other two criteria. The phase variance stability classifies approximately 2–3% of the initial population as PS_f while the proportion is about ten times higher for the standard deviation of the slope.

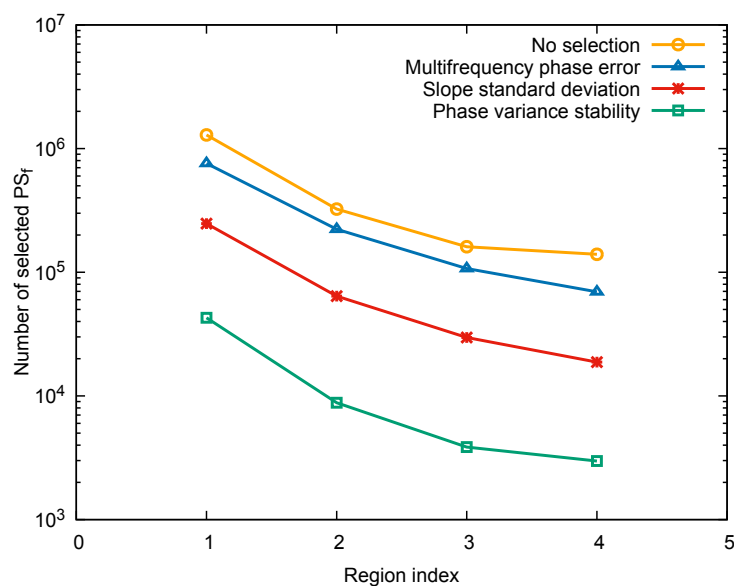


Figure 7. Number of selected PS_f for regions 1 to 4 using the different detection criteria. The y -axis is on a logarithmic scale.

All four of the selection methods provide the same phase ambiguities corrections of the disconnected regions. These corrections are listed in Table 2. As indicated before, the expected relative phase-offsets are given in Table 1. Based on the validation strategy proposed in the previous section, we verify that our results are consistent with these values. Even though the four situations give similar measurements, the precision of the result is not the same. Looking at the histogram of the normalized distribution of the phase-offset estimates in region 3 (Figure 8), we observe that the dispersion of the distribution varies from one criterion to the other, but the modes of the distributions

are indeed the same. When no selection of PS_f is applied, the distribution is spread over a large range of values with a low probability for the mode bin. This behavior is similar for histograms over all the other regions. The quality of the results without selection criterion applied is quantified by a W/H ratio of about 45–50 for most regions, with the highest value of 85 for region 4 (see Table 3). The larger dispersion in region 4 is probably due to the large uncorrelated patch present in the split-band phase. Those targets are most probably unstable and they are not discriminated in this case. The W/H aspect ratio is lowered when the multifrequency phase error criterion is applied to select stable pixels. In this case, the contrast between the dispersion in region 4 and the three others is significantly reduced.

Table 2. Phase-offset corrections for artificially disconnected regions.

Computed Phase-Offset	Cycles
n_1	-3
n_2	-2
n_3	-3
n_4	-2

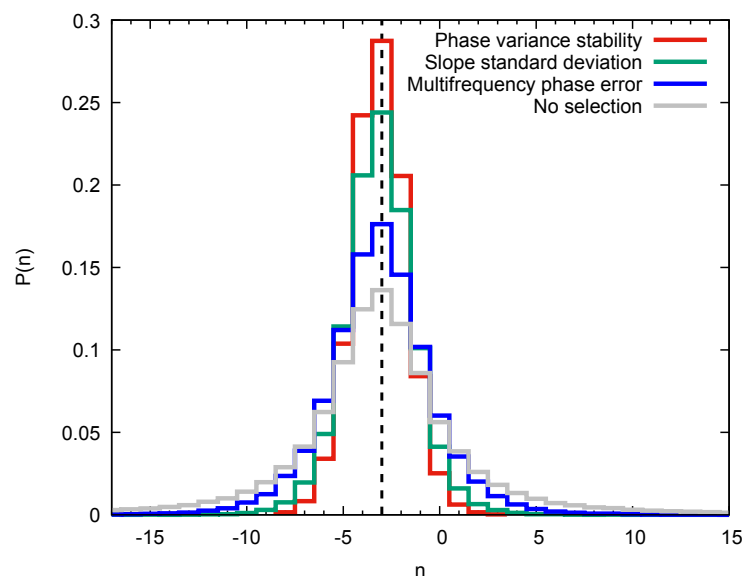


Figure 8. Normalized histograms of the estimated phase-offset values n for region 3. The gray line histogram represents the case where no selection of PS_f is applied. For other cases, the PS_f population is selected using three different criteria. The vertical dashed line indicates the expected phase ambiguity. Similar figures are obtained for the three other regions.

Table 3. Ratio W/H of the phase-offsets distributions of artificially disconnected regions.

PS_f Selector	Region 1	Region 2	Region 3	Region 4
	W/H	W/H	W/H	W/H
None	54	43	43	85
σ_v	25	26	25	30
σ_s	12	14	12	13
$\sigma_{\phi_i}^2$	8	9	8	9

Let us now consider our two new selection criteria: with the standard deviation of the slope, the aspect ratio is still improved by a factor 2. The best ratio is, however, obtained by using the phase variance stability criteria. Similar results are found for the other areas. The W/H ratio seems to be correlated with the population of frequency-persistent scatterers: the smallest the number of selected pixels, the lowest the aspect ratio. Among the PS_f selection criteria considered in this study, the phase variance stability appears to be the most efficient. However, when applied to a less favorable case, e.g., to images with a smaller bandwidth or small disconnected areas, this criterion can be too restrictive and the population of selected PS_f will be too limited to estimate the phase ambiguity reliably. In such cases, the standard deviation of the slope is a satisfactory alternative.

After validation of the procedure, the SBInSAR-assisted phase unwrapping is applied to the ensemble of the naturally and artificially disconnected regions of the unwrapped phase. Using the phase variance stability to detect stable targets, 33 regions out of 1796 are corrected while, using the standard deviation of the slope, we reach an amount of 74 regions. Let us remind that a region will be corrected if it holds at least 10 PS_f and if the phase-offset mode is unique. During the test on the artificially disconnected areas, we observed that the phase variance stability selected fewer targets than the standard deviation of the slope in a given region. We reach a similar conclusion for the naturally disconnected areas (Figure 9). It is interesting to note that the majority of the pixels identified by the phase variance stability are also identified by the standard deviation of the slope. Less than 1% of the PS_f population is selected by the phase variance stability only.

For regions with a PS_f population larger than 30 pixels, we observe in Figure 10 that the mode of the phase-offset distribution represents approximately 20–30% of the detected PS_f for the standard deviation of the slope and a slightly higher value of 25–35% for the phase variance stability. Regions with smaller population of stable targets can exhibit even larger values. The regions with an occurrence of the mode below 20% of the PS_f population are an exception, whatever the detection criterion.

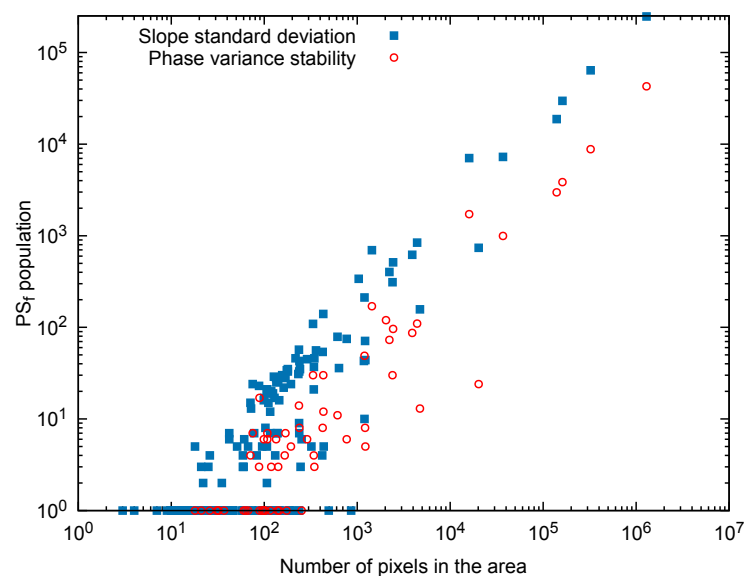


Figure 9. PS_f population as a function of the size of the area, for both artificially and naturally disconnected areas. Regions with no PS_f are not represented. Axes are in logarithmic scale.

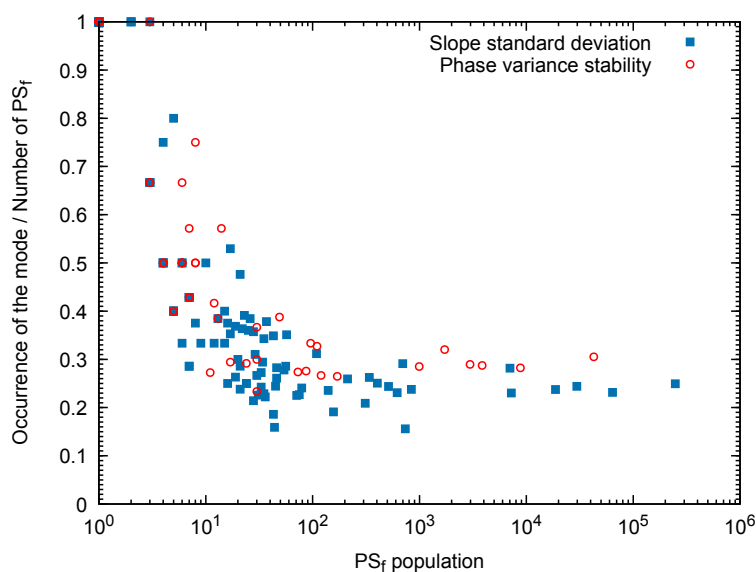


Figure 10. Probability of the mode of the phase-offset distribution as a function of the amount of selected PS_f in a given region, for both artificially and naturally disconnected areas. Regions with multiple modes are not represented. The x -axis is on the logarithmic scale.

As it can be seen in Figure 9, whose axes are in logarithmic scale, there seems to be no relationship between the size of a patch and the PS_f population. The stable nature of a target is probably related to its intrinsic characteristics and/or the geometry of observation, which causes a heterogeneous distribution of the targets across the scene. Since the population of stable targets is the key point to determine the phase ambiguity, and it cannot be related to the initial population of a given region, it is not possible to define the minimum size of an area where the SBInSAR-assisted phase unwrapping can be applied. However, we observe that when the standard deviation of the slope is considered, the largest region with no PS_f at all is made of less than 400 pixels. For the phase variance stability criterion, the largest region has a size of 3665 pixels, but most of them contain less than 500 pixels.

5. Conclusions

This study has presented a probabilistic approach based on Split-Band Interferometry to correct the local phase ambiguities introduced during phase unwrapping of classical InSAR process. The applicability and potential of the proposed approach have been demonstrated on a TerraSAR-X pair of images over Copahue volcano, showing steep topography and local loss of coherence. The corrections have been computed for artificially disconnected areas, allowing an indirect validation of the results. We have shown that the SBInSAR-assisted phase unwrapping is efficient for X-band images with a large range bandwidth like spotlight images.

We suggested two new criteria to select frequency-persistent scatterers, one based on the phase variance stability and the other on the slope standard deviation. Both were tested and compared to the multifrequency phase error based on the aspect ratio of the offsets distribution. With each one of the three selectors, the expected corrections were retrieved. However, the phase variance stability showed more precise estimates, though the standard deviation of the slope gave satisfactory results. Both appeared to be more efficient than the multifrequency phase error.

When we applied the SBInSAR-assisted phase unwrapping to naturally disconnected regions as well, without validation of the phase-offset correction, we noted a factor larger than two between the amount of regions corrected using the stability of the phase variance and using the standard deviation of the slope. The phase variance stability appears to be too demanding for small regions. So far, no

correlation has been observed between the size of a patch and the number of stable targets detected in this patch. As a consequence, the minimum size of a corrigible region could not be determined.

Conventional phase unwrapping algorithms, such as SNAPHU [19–21], propose deformation mode to handle abrupt deformations or normalization options to level the phase of close areas. In this case, the consequence may be that the phase ambiguity is not an integer number of cycles anymore and an a priori estimation of the deformation gradient might be necessary. With the SBInSAR-assisted phase unwrapping, disconnected regions are reconnected by correcting an offset that is an integer number of cycles, preserving thus phase information integrity. Moreover, this leveling of the phase is done by exploiting only the spectral information of SAR images and does not require additional data, like on-ground measurements (e.g., GPS). The drawback of this approach is that it will not reconnect small regions because of the need for a sufficient population of stable targets. Additionally, spectral decomposition is demanding regarding memory and computing time. However, this technique keeps all its interest for practical cases with steep topography, local coherence losses, geometrical distortions or high-gradient deformations leading to phase unwrapping issues.

Future work will focus on the applicability of the method to images with smaller bandwidth and the definition of the best selector of PS_f in a standard case. Decreasing the bandwidth to 100–150 MHz, we expect a reduced population of PS_f due to the loss of resolution but still reasonable results. In addition, the method has been validated on disconnected areas with an important initial population (>105 pixels) and consequently with a higher probability to include stable targets. The next step will be to apply and validate it for smaller regions. Finally, due to the dependency of the split-band phase accuracy on the frequency, we expect better results with C-band or L-band data. In the future, the SBInSAR-assisted phase unwrapping will be tested on Sentinel-1 data.

Acknowledgments: This work was carried out in the framework of the MUZUBI (MUlti-Zone phase Unwrapping using advanced split-Band Interferometry) and RESIST (REmote Sensing and In Situ detection and Tracking of geohazards) projects funded respectively by the Belgian Science Policy contracts Nos. SR/00/324 and SR/00/305. Test data were provided by the DLR in the framework of the TanDEM-X Science Phase announcement of opportunity for the project "Split-Band InSAR monitoring of Virunga and Copahue volcanoes using TanDEM-X."

Author Contributions: Ludivine Libert developed the theoretical aspects of the frequency-persistent scatterers selection and the SBInSAR-assisted phase unwrapping approach, and processed the data. Dominique Derauw developed the split-band processor and provided technical support for its use. Nicolas d'Oreye, Christian Barbier and Anne Orban participated to the data analysis and interpretation. All of the authors participated in editing and reviewing the manuscript.

Conflicts of Interest: The authors declare no conflict of interest.

Abbreviations

The following abbreviations are used in this manuscript:

PS_f	Frequency-Persistent Scatterer(s)
SAR	Synthetic Aperture Radar
InSAR	Synthetic Aperture Radar Interferometry
SBInSAR	Split-Band Interferometry
DEM	Digital Elevation Model

References

1. Bovenga, F.; Giovazzo, V.M.; Refice, A.; Nitti, D.O.; Veneziani, N.V. Interferometric Multi-Chromatic Analysis of High Resolution X-Band Data. In Proceedings of the Fringe 2011 Workshop, Frascati, Italy, 19–23 September 2011.
2. Veneziani, N.; Bovenga, F.; Refice, A. A Wide-Band Approach to the Absolute Phase Retrieval in SAR Interferometry. *Multidimens. Syst. Signal Process.* **2003**, *14*, 183–205.
3. Bovenga, F.; Giovazzo, V.M.; Refice, A.; Veneziani, N. Multichromatic Analysis of InSAR Data. *IEEE Trans. Geosci. Remote Sens.* **2013**, *51*, 4790–4799.
4. Bovenga, F.; Rana, F.M.; Refice, A.; Veneziani, N. Multichromatic Analysis of Satellite Wideband SAR Data. *IEEE Geosci. Remote Sens. Lett.* **2014**, *11*, 1767–1771.

5. De Rauw, D.; Kervyn, F.; d'Oreye, N.; Albino, F.; Barbier, C. Split-Band Interferometric SAR Processing Using TanDEM-X Data. In Proceedings of the FRINGE'15: Advances in the Science and Applications of SAR Interferometry and Sentinel-1 InSAR Workshop, Frascati, Italy, 23–27 March 2015.
6. Bovenga, F.; Giacobozzo, V.M.; Refice, A.; Veneziani, N.; Vitulli, R. Multi-Chromatic Analysis of InSAR Data: Validation and Potential. In Proceedings of the Fringe 2009, Frascati, Italy, 30 November–4 December 2009.
7. Bovenga, F.; Derauw, D.; Rana, F.M.; Barbier, C.; Refice, A.; Veneziani, N.; Vitulli, R. Multi-Chromatic Analysis of SAR Images for Coherent Target Detection. *Remote Sens.* **2014**, *6*, 8822–8843.
8. Ferretti, A.; Prati, C.; Rocca, F. Permanent Scatterers in SAR Interferometry. *IEEE Trans. Geosci. Remote Sens.* **2001**, *39*, 8–20.
9. Derauw, D.; Orban, A.; Barbier, C. Wide Band SAR Sub-Band Splitting and Inter-Band Coherence Measurements. *Remote Sens. Lett.* **2010**, *1*, 133–140.
10. Rosen, P.A.; Hensley, S.; Chen, C. Measurement and mitigation of the ionosphere in L-band Interferometric SAR data. In Proceedings of the 2010 IEEE Radar Conference, Arlington, VA, USA, 10–14 May 2010; pp. 1459–1463.
11. Furuya, M.; Suzuki, T.; Derauw, D. A step-by-step recipe of band splitting technique for isolation of ionospheric signal in L-band InSAR data. In Proceedings of the AGU Fall Meeting, San Francisco, CA, USA, 12–16 December 2016.
12. Schreiber, R.; Moreira, A. Coregistration of Interferometric SAR Images Using Spectral Diversity. *IEEE Trans. Geosci. Remote Sens.* **2000**, *38*, 2179–2191.
13. Jiang, H.; Feng, G.; Wang, T.; Bürgmann, R. Toward full exploitation of coherent and incoherent information in Sentinel-1 TOPS data for retrieving surface displacement: Application to the 2016 Kumamoto (Japan) earthquake. *Geophys. Res. Lett.* **2017**, *44*, 1758–1767.
14. Naranjo, J.A.; Polanco, E. The 2000 AD eruption of Copahue Volcano, Southern Andes. *Rev. Geol. Chile* **2004**, *31*, 279–292.
15. Tamburello, G.; Agosto, M.; Caselli, A.; Tassi, F.; Vaselli, O.; Calabrese, S.; Rouwet, D.; Capaccioni, B.; Napoli, R.D.; Cardellini, C.; et al. Intense magmatic degassing through the lake of Copahue volcano, 2013–2014. *J. Geophys. Res. Solid Earth* **2015**, *120*, 6071–6084, doi:10.1002/2015JB012160.
16. Fournier, T.J.; Pritchard, M.E.; Riddick, S.N. Duration, magnitude, and frequency of subaerial volcano deformation events: New results from Latin America using InSAR and a global synthesis. *Geochem. Geophys. Geosystems* **2010**, *11*, doi:10.1029/2009GC002558.
17. Velez, M.L.; Euillades, P.; Caselli, A.; Blanco, M.; Díaz, J.M. Deformation of Copahue volcano: Inversion of InSAR data using a genetic algorithm. *J. Volcanol. Geotherm. Res.* **2011**, *202*, 117–126.
18. Goldstein, R.M.; Zebker, H.A.; Werner, C.L. Satellite radar interferometry: Two-dimensional phase unwrapping. *Radio Sci.* **1988**, *23*, 713–720.
19. Chen, C.W.; Zebker, H.A. Network approaches to two-dimensional phase unwrapping: intractability and two new algorithms. *J. Opt. Soc. Am. A* **2000**, *17*, 401–414.
20. Chen, C.W.; Zebker, H.A. Two-dimensional phase unwrapping with use of statistical models for cost functions in nonlinear optimization. *J. Opt. Soc. Am. A* **2001**, *18*, 338–351.
21. Chen, C.W.; Zebker, H.A. Phase unwrapping for large SAR interferograms: Statistical segmentation and generalized network models. *IEEE Trans. Geosci. Remote Sens.* **2002**, *40*, 1709–1719.

